

Evaluation of resonances via AAA rational approximation of randomly scalarized boundary integral resolvents

Oscar P. Bruno*

Manuel A. Santana*

Lloyd N. Trefethen[†]

May 31, 2024

Abstract

This paper presents a novel algorithm, based on use of rational approximants of randomly scalarized boundary integral resolvents, for the evaluation of acoustic and electromagnetic resonances in open and closed cavities; for simplicity we restrict treatment to cavities in two-dimensional space. The desired open cavity resonances (also known as “eigenvalues” for interior problems, and “scattering poles” for exterior and open problems) are obtained as the poles of associated rational approximants; both the approximants and their poles are obtained by means of the recently introduced AAA rational-approximation algorithm. In fact, the proposed resonance-search method applies to any nonlinear eigenvalue problem (NEP) associated with a given function $F : U \rightarrow \mathbb{C}^{n \times n}$, wherein a complex value k is sought for which $F_k w = 0$ for some nonzero $w \in \mathbb{C}^n$. For the cavity problems considered in this paper, F_k is taken as a spectrally discretized version of a Green function-based boundary integral operator at spatial frequency k . In all cases, the scalarized resolvent is given by an expression of the form $u^* F_k^{-1} v$, where $u, v \in \mathbb{C}^n$ are fixed random vectors. A variety of numerical results are presented for both scattering resonances and other NEPs, demonstrating the accuracy of the method even for high frequency states.

1 Introduction

We are concerned with the problem of evaluation of resonances supported by open and closed cavities and other scattering structures, which are obtained as solution pairs (u, k) of the eigenvalue problem

$$\Delta u + k^2 u = 0 \tag{1}$$

with eigenfunction u and eigenvalue $-k^2$, posed on an interior or exterior domain Ω , with homogeneous boundary conditions of e.g. Dirichlet, Neumann, or other types. Once approximated by discretized versions of the problem’s boundary integral operators (which is done in this paper on the basis of the open- and closed-curve integral equation algorithms [6,17], see also [7]), the resonance-search problem is reduced to the solution of a related Nonlinear Eigenvalue Problem (NEP) for a certain function $F : U \rightarrow \mathbb{C}^{n \times n}$, wherein a complex value k is sought for which

$$F_k w = 0 \quad \text{for some nonzero } w \in \mathbb{C}^n. \tag{2}$$

This contribution focuses on scattering problems, for which the function F in (2) provides a discrete approximation of the associated boundary-integral operator. However the method is general and, indeed, other NEPs unrelated to boundary integral operators are considered in this paper as well.

*Computing and Mathematical Sciences, California Institute of Technology, Pasadena, CA, 91125 USA, obruno@caltech.edu, msantana@caltech.edu

[†]School of Engineering and Applied Sciences, Harvard University, Cambridge, MA 02138 USA (trefethen@seas.harvard.edu)

The proposed approach seeks the desired resonant values k , for which (2) holds, as poles of the randomly scalarized resolvent

$$S(k) = u^* F_k^{-1} v, \quad \text{where } u, v \in \mathbb{C}^n \quad \text{are fixed random vectors} \quad (3)$$

The desired resolvent poles are obtained as poles of rational approximants of (3); both the rational approximants and their poles are produced numerically by means of the recently introduced AAA rational-approximation algorithm [22]. The overall approach is simple to implement and rapidly convergent, and it requires limited computational cost besides the embarrassingly parallelizable evaluation of the scalarized resolvent at various wavenumbers k . A variety of numerical results presented in this paper demonstrate the character of the proposed approach: the method yields highly accurate approximations of scattering resonances and solutions of other NEPs, even in cases involving high frequencies.

A significant literature has developed in recent years in connection with the solution of NEPs. General solution methods include root finding methods, contour integration methods, and methods based on approximations of F_k with an NEP whose eigenvalues can be found easily (see the survey [15] and references therein), all of which have been applied to the computation of resonances [2, 3, 12, 21, 24, 26]. Recently, methods employing AAA have been developed for the nonlinear eigenvalue problem [16, 23], and specifically, the use of AAA applied to the scalar function $u^* F(k)^{-1} v$ was considered in [13, 14]. However in these contexts AAA is used in the construction of a linear eigenvalue problem whose solutions approximate the eigenvalues of the NEP, whereas we propose direct use of the poles of the AAA rational approximation of the scalar function S to solve the NEP.

This paper is organized as follows. Sections 2 and 3 review the integral-equation framework and the associated numerical schemes used in this paper to represent solutions of the Helmholtz equation (1) for open and closed two-dimensional domains. Section 4 then provides a brief description of the AAA algorithm. The overall proposed approach for the solution of NEPs is then presented in Section 5. A variety of numerical experiments illustrating the proposed methodology and a few concluding remarks, finally, are presented in Sections 6 and 7.

2 Eigenvalue problems, Green Functions and Integral Operators

We consider eigenvalue problems of the form (1), posed in open two dimensional spatial domains Ω with smooth boundaries Γ , and with homogeneous boundary conditions on Γ . Three types of spatial domains are considered in this paper, namely, domains Ω equal to: (a) The complement Γ^c of an open arc Γ in \mathbb{R}^2 ; (b) The region interior to a closed curve Γ in \mathbb{R}^2 ; and, (c) The region exterior to a closed curve Γ in \mathbb{R}^2 . For definiteness this paper restricts attention to eigenvalue problems under homogeneous Dirichlet boundary conditions

$$u|_{\Gamma} = 0 \quad (4)$$

for each of the domain-types mentioned above. Homogeneous Neumann and Zaremba boundary conditions can be handled similarly [1, 2, 17].

Our treatment of the problem (1)–(4) is based on use of the two dimensional Helmholtz Green function $G_k(x, y) := \frac{i}{4} H_0^1(k|x - y|)$ (where H_0^1 denotes the Hankel function of the first kind of order 0) and the associated single-layer potential representation

$$u(x) = \int_{\Gamma} G_k(x, y) \psi(y) ds_y, \quad x \in \Omega, \quad (5)$$

of the eigenfunction u in terms of a surface density ψ . In view of the well known [9, 19] continuity of the single layer potential $u = u(x)$ as a function of $x \in \mathbb{R}^2$, up to and including Γ , we consider the boundary integral operator $F_k : H^{-1/2}(\Gamma) \rightarrow H^{1/2}(\Gamma)$ (resp. $F_k : \tilde{H}^{-1/2}(\Gamma) \rightarrow H^{1/2}(\Gamma)$) given by the expression

$$F_k[\psi](x) = \int_{\Gamma} G_k(x, y) \psi(y) ds_y, \quad x \in \Gamma \quad (6)$$

on a closed (resp. open) smooth curve Γ ; see [19] and [17] and references therein for detailed definitions of the Sobolev spaces $H^{\pm 1/2}$ and $\tilde{H}^{1/2}$ relevant to the closed and open-arc single layer operators, respectively.

As suggested above, the k -dependent operator (6) can be used to tackle the interior, exterior and open-arc eigenvalue problems under consideration. Indeed, for any smooth open arc or closed curve Γ and for any given density function ψ defined on Γ , we have [19] (i) The function u given by the representation formula (5) is a solution of equation (1) for all $x \in \Gamma^c$; and, (ii) The function $u \neq 0$ satisfies the Dirichlet boundary condition (4) if and only if $\psi \neq 0$ is a solution of the equation $F_k[\psi] = 0$. It can accordingly be shown that the resolvent operator $(F_k)^{-1}$ is an analytic function of k for $\Im k > 0$, and that that given a complex number $k = \mu$ with $\Im \mu \leq 0$, the number $-\mu^2$ is an eigenvalue of the problem (1)–(4) if and only if the value $k = \mu$ is a pole of the resolvent operator $(F_k)^{-1}$ as a function of k . This fact is established in [25, Prop. 7.10] for closed-curve interior problems (for which μ in the lower half-plane $\Im \mu \leq 0$ must actually be real) and for closed-curve exterior problems (for which μ must satisfy $\Im \mu < 0$). As indicated in what follows, the corresponding result for open-arc problems can be established along lines similar to those in [25, Prop. 7.10].

A critical element in the extension of these results to the open-arc case is the injectivity of the mapping $\psi \rightarrow u$, which, according to equation (5), maps functions defined on Γ to functions defined in \mathbb{R}^2 . The corresponding closed-curve injectivity result for the exterior problem is established in [25] by showing that if ψ satisfies the equation $F_k(\psi) = 0$, then the associated function u given by (5) is a Laplace eigenfunction in the interior of Γ and that, therefore, the corresponding eigenvalue $-\mu^2$ must be real, and by subsequently making use of the jump relations for the single- and double-layer potentials across Γ . The corresponding closed-curve result for the interior problem is established similarly. For the open-arc problem we have no equivalent of the interior region, but the injectivity result can be established nevertheless, simply by using the jump relation for the normal derivative of the single-layer potential. The equivalence between Laplace eigenvalues $-\mu^2$ with μ in the lower-half plane and poles $k = \mu$ of the resolvent $(F_k)^{-1}$ then follows for the open arc case in a manner analogous to that put forth in [25, Sec. 7] by relying on the second-kind formulation for open problems introduced in [6, 17].

In sum, noting that, without loss of generality, the search for values of k satisfying the eigenvalue problem (1)–(4) may be restricted to the lower half-plane $\Im k \leq 0$, the eigenvalues may be sought as real poles $k = \mu$ of the resolvent operator $(F_k)^{-1}$ for the eigenvalue problem in the interior of a closed curve Γ , and as complex poles $k = \mu$ of the same operator, with $\Im \mu < 0$, for either the eigenvalue problem in the exterior of a closed curve Γ or for the complement of an open arc Γ . The associated eigenfunctions u then result via equation (5) with density (or, for multiple eigenvalues, densities) ψ in the nullspace of the operator F_k . In other words, the integral equation setting just described reduces the eigenvalue problem (1)–(4) for interior and exterior closed-curve and open arc problems to an NEP for the single-layer operator (6) with values of k restricted to the lower half plane.

3 Numerical Instantiation of the Integral Operator F_k

The numerical implementations utilized in this paper are based on the discretization methods presented in [10, Sec. 3.6] (resp. [6, Secs. 3.2, 5.1]) for closed (resp. open) curves. For simplicity, our computational examples restrict attention to smooth curves Γ and boundary conditions of Dirichlet type, although related methods are available [1, 6, 10] that enable corresponding treatments for non-smooth boundaries [1, 10] as well as Neumann, Robin and Zaremba boundary conditions [1, 6]. As indicated in [6], in particular, the numerical implementation of the integral operator (6) for open arcs Γ requires consideration of the edge singularities that are incurred by the solutions ψ of problems of the form $F_k[\psi] = f$ even for functions f defined on Γ which do not contain such singularities.

Algorithm 1: Basic Algorithm

```
1 Select a set  $Z_N = \{k_1, \dots, k_N\} \subset \mathcal{C}$ 
2 Choose random vectors  $u, v \in \mathbb{C}^n$ 
3 for  $j = 1, \dots, N$  do
4    $s_j = u^* F(k_j)^{-1} v$ 
5 end
6 Compute the rational approximant  $r(z)$  associated with the set  $\{(k_j, s_j) \mid s_j = S(k_j), j = 1, \dots, N\}$ 
   using the AAA algorithm
7 Return the poles of  $r(z)$  inside  $\mathcal{C}$ 
```

For both, open- and closed-curve problems the methods [6, 10] discretize the single layer operator F_k on the basis of Nyström-type methodologies—utilizing a sequence of points along the curve Γ which are used for the purposes of both integration and enforcement of the equation. For closed curves Γ the discretization is produced as the image under the curve parametrization of a uniform grid in the parameter interval $[0, 2\pi]$; in the case of open curves the discretization results as the image of a Chebyshev mesh in the parameter interval $[-1, 1]$. In both cases the unknown functions ψ are expressed in terms of Fourier-based expansions in the parameter intervals, which are then integrated termwise by reducing each integrated term to evaluation of explicit integrals. The edge singularities of the function ψ in the open-arc case are tackled by explicitly factoring out the singular term: using a smooth parametrization $\mathbf{r} = \mathbf{r}(t)$ of the open curve Γ ($-1 \leq t \leq 1$) and writing $\psi(\mathbf{r}(t)) = \phi(\mathbf{r}(t))/\sqrt{1-t^2}$, it follows that ϕ is a smooth function. Upon introduction of a cosine change of integration variables two desirable effects occur, namely, the function ϕ is converted into a periodic and even function which may be expanded in a cosine series with high accuracy, and, at the same time, the square root term in the denominator is cancelled by the Jacobian of the change of variables. The method is completed by exploiting explicit expressions for the integral of products of a logarithmic kernel and the cosine Fourier basis functions. As illustrated in [6] and other contributions mentioned above, these methodologies can produce scattering solutions with accuracies near machine precision on the basis of relatively coarse discretizations, even for configurations involving high spatial frequencies.

Algorithm 2: Adaptive Algorithm

Input: Eigenvalues e from Algorithm 1 applied to a curve \mathcal{C}

```
1 Function eigadaptive( $e, \mathcal{C}$ )
2   Partition the interior of  $\mathcal{C}$  into sets with boundary  $C_i$ 
3   for each  $C_i$  do
4     Compute  $n_i$  the number of eigenvalues  $e$  inside  $C_i$ 
5     Compute eigenvalues  $\tilde{e}$  from Algorithm 1 applied to  $C_i$ 
6     Compute  $\tilde{n}_i$  the number of eigenvalues  $\tilde{e}$  inside  $C_i$ 
7     if  $n_i = \tilde{n}_i$  then
8       return  $\tilde{e}$ 
9     else
10      return eigadaptive( $\tilde{e}, C_i$ )
11   end
```

In particular, these procedures produce highly accurate numerical approximations of the integral operator F_k in (5)—which we exploit in the context of this paper to produce accurate numerical evaluations of eigenvalues and eigenfunctions. As indicated in Section 5, the poles of (a randomly scalarized version of) this integral operator, which, per the discussion in Section 2, correspond to Laplace eigenvalues in the various cases considered, are then obtained as poles of associated AAA rational approximants. The corresponding eigenfunctions are obtained via consideration of a Gaussian elimination-based de-singularization

procedure described in Section 5. For added accuracy, the methods in that section propose two alternatives, namely, the use of either iterated AAA rational approximants on one hand, and application of the secant method after an initial evaluation of poles via the AAA approach, on the other hand. In practice we have observed that, without exceptions, accuracies near machine precision are obtained for both eigenvalues and eigenfunctions on the basis of the overall proposed methodology; a few related illustrations are presented in Section 6.

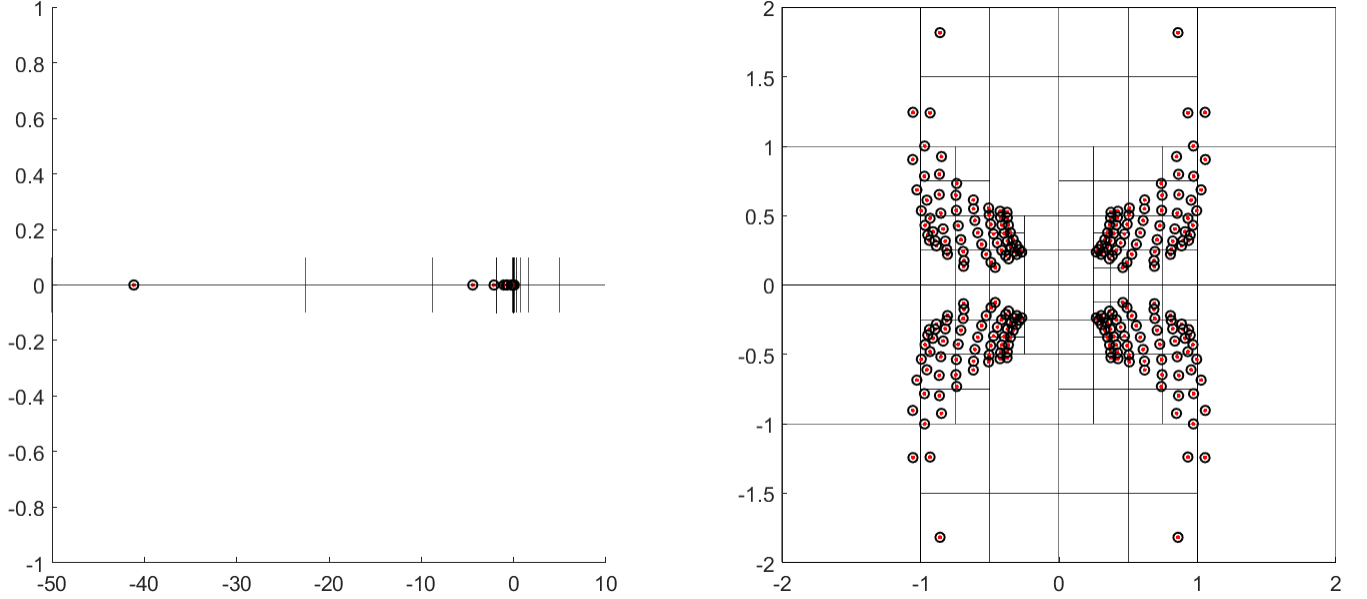


Figure 1: Demonstration of Algorithm 2 on two problems from the NLEVP set [4]. In both panels red points represent exact eigenvalues and black circles represent eigenvalues produced by the proposed numerical method. Black lines represent divisions related to the recursive version of the algorithm. Left panel: The CD player problem, for which all 60 eigenvalues were found to at least 7 digits. Right: The butterfly problem, for which all 256 eigenvalues were found to at least 10 digits. Accuracy near machine precision was subsequently obtained by increasing the discretization in each subregion or by using methods refinement secant- or AAA-based methods described in Sections 5 and 6.2

4 Rational Approximants and the AAA Algorithm

The AAA algorithm is a greedy procedure for the construction of a rational approximant to a given complex-valued function f on the basis of its values on an N -point set $Z_N \subset \mathbb{C}$. (Full details can be found in [22].) Given the set $\{(z, f(z)) \mid z \in Z\}$, the algorithm proceeds by selecting a sequence of points $z_j \in Z$, starting with some point z_1 , which in principle can be selected arbitrarily, but which the Matlab implementation [11] takes as a $z \in Z_N$ for which the function value $f(z)$ is farthest from the mean of the set $\{f(z) \mid z \in Z\}$. The remaining points are then selected inductively. Once points $z_j \in Z_N$ ($1 \leq j \leq m$) have been chosen, for a suitably chosen vector $w^m = (w_1^m, \dots, w_m^m)$ of complex weights w_j^m satisfying $\sum |w_j|^2 = 1$, the procedure to obtain z_{m+1} starts by constructing the barycentric-form rational function

$$r(z) = \frac{n^m(z)}{d^m(z)} = \sum_{j=1}^m \frac{w_j^m f_j}{z - z_j} \bigg/ \sum_{j=1}^m \frac{w_j^m}{z - z_j}, \quad (7)$$

where, as suggested by the notation used, $n^m(z)$ and $d^m(z)$ denote the numerator and denominator in the right-hand expression in (7). The vector w^m is selected as follows: calling $A_m = \{(\tilde{w}_1, \dots, \tilde{w}_m) \in \mathbb{C}^m \mid \sum |\tilde{w}_j|^2 = 1\}$, w^m is defined as the minimizer of the least-squares problem

$$w^m = \arg \min_{\tilde{w} \in A_m} \sum_{z \in Z_N^m} |f(z)d_{\tilde{w}}(z) - n_{\tilde{w}}(z)|^2,$$

where $Z_N^m = Z_N \setminus \{z_j \mid j = 1, \dots, m\}$, $n_{\tilde{w}}(z) = \sum_{j=1}^m \frac{\tilde{w}_j f_j}{z - z_j}$ and $d_{\tilde{w}}(z) = \sum_{j=1}^m \frac{\tilde{w}_j}{z - z_j}$. Once the minimizer w^m has been computed, z_{m+1} is defined as the point $z \in Z_N^m$ for which $|f(z) - n^m(z)/d^m(z)|$ is maximum. The algorithm terminates when this maximum is less than or equal to a specified tolerance, and the last rational function (7) obtained as part of the z_j selection process provides the desired rational approximant.

All of the numerical illustrations presented in this paper utilize AAA implementation included with Chebfun [11].

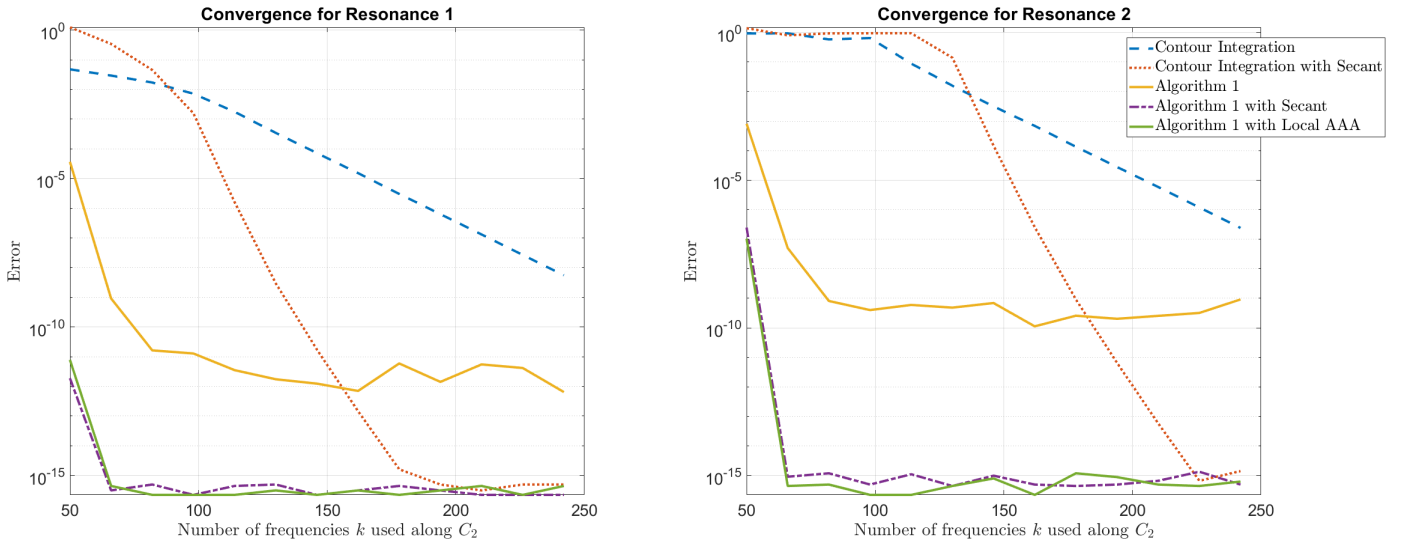


Figure 2: Comparison of Algorithm 1 to the contour integration algorithm on the problem of evaluation of scattering poles outside the unit disc. The errors on the left and right panels are evaluated by comparison with the exact Hankel function roots near $1.3080 - 1.6818i$ and $2.2044 - 1.9782i$, respectively. The curves labeled “with secant” were obtained by following the initial AAA eigenvalue determination by four iterations of the secant method. For the curve labeled “with local AAA”, four points were sampled on a circle of radius $1e - 5$ around the initial AAA approximation of the pole together with a degree 1 rational approximant. To avoid underflow the maximum between the error and machine precision is plotted in all cases.

5 Solution of NEPs

The discussion in Sections 2 and 3 reduces the eigenvalue problem (1)–(4) to NEPs for the single-layer operator (6) (and the corresponding discrete approximate operator introduced in Section 3), with values of k restricted to the lower half plane. This section presents numerical algorithms for the solution of this NEP and, indeed, of general NEPs for which the resolvent operator $(F_k)^{-1}$ is a meromorphic function of k .

As indicated in Section 1, the proposed NEP algorithm obtains the eigenvalues k as the poles of the AAA rational approximants associated with the randomly scalarized resolvent (3). Thus, a simple algorithm for the computation of the eigenvalues contained in the interior of a curve \mathcal{C} in the complex plane proceeds

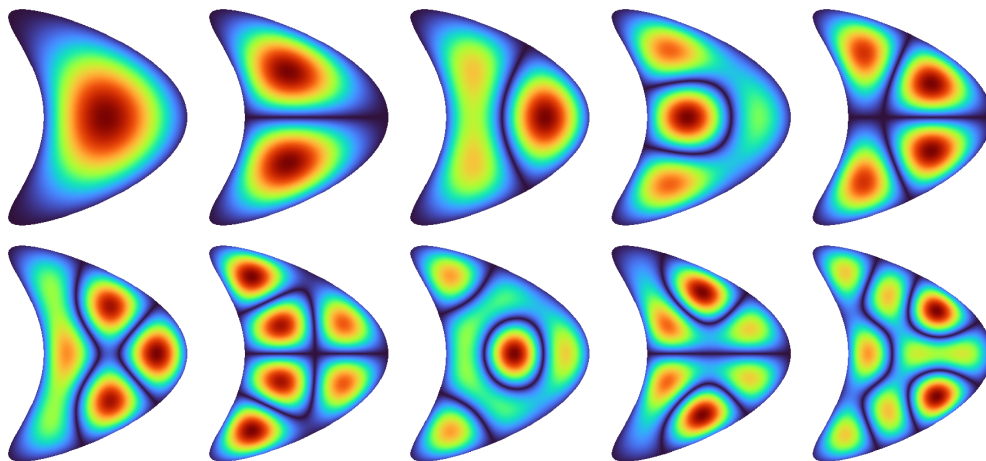


Figure 3: Low-frequency interior eigenvalue problems mentioned in section 6.3: the first ten interior eigenfunctions for the kite-shaped domain. The associated frequencies k are displayed in the left column of Table 1.

by first evaluating the scalarized resolvent $S = S(k)$ at a suitably selected set $Z_N = \{k_1, \dots, k_N\}$ along \mathcal{C} to obtain the set $\{(k_j, s_j) \mid s_j = S(k_j), j = 1, \dots, N\}$. Using this set of pairs, a rational approximant $r = r(k)$ is obtained by applying the AAA algorithm, and the poles of $r(k)$ within \mathcal{C} are returned as approximations of the eigenvalues of $F(k)$. In the case where the eigenvalues are on the real line, the curve in the complex plane can be replaced with a real interval, and eigenvalues can be recovered as poles of the rational approximant with sufficiently small imaginary part. A corresponding pseudo-code is presented in Algorithm 1.

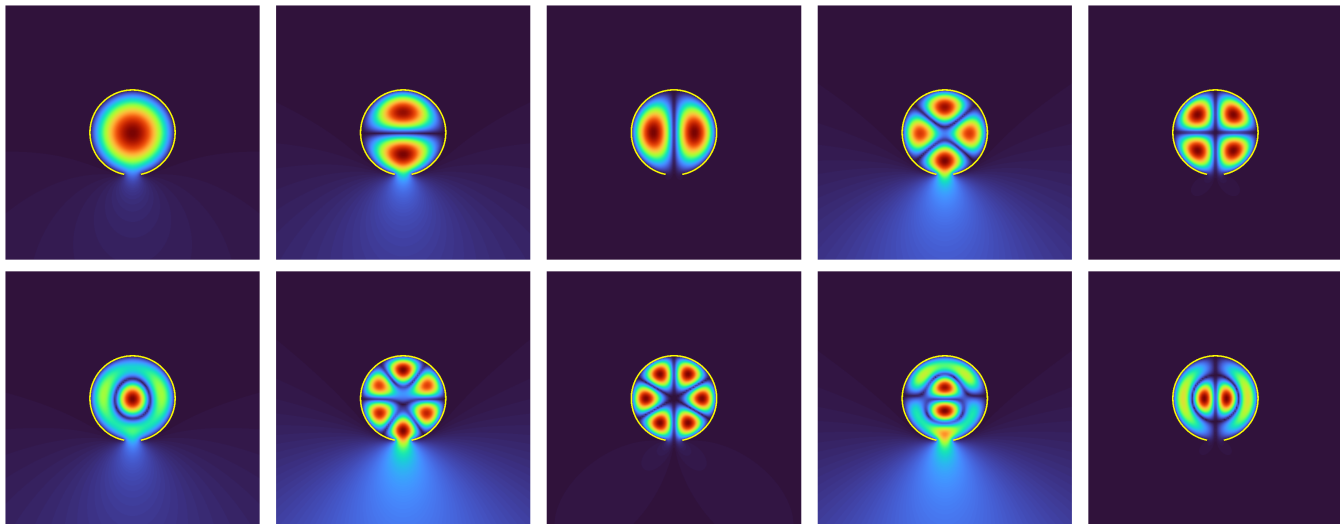


Figure 4: Low-frequency open arc eigenproblems discussed in section 6.3: the first ten scattering poles of the open circle with imaginary part of the eigenvalue less than $-0.2i$ (ordered left-to-right and top-to-bottom with increasing values of the real part of the frequency). The associated frequencies k are displayed in the right column of Table 1.

Algorithm 1 works best when there are not too many eigenvalues inside \mathcal{C} , since, indeed, in order to avoid rational approximants that produce spurious poles along the complex contour \mathcal{C} it is preferable to utilize the AAA algorithm with relatively small values of m . But approximants with small values of m

Kite	Open Circle
2.209856180349	2.391850921204 - 0.000866833533i
3.215653682128	3.785851440218 - 0.007551333804i
3.528868275787	3.831519839558 - 0.000000810935i
4.303831479675	5.066410135738 - 0.022753855105i
4.371112240590	5.134599571714 - 0.000011845979i
4.906513621606	5.486798760828 - 0.010839713761i
5.291183742145	6.297659940294 - 0.044691641691i
5.461743432329	6.377232306043 - 0.000071959651i
5.736410337307	6.923647500434 - 0.056416692369i
6.172352448525	7.015195622517 - 0.000013514954i

Table 1: Computed frequencies k (listed top-to-bottom in this table) such that $-k^2$ is an eigenvalue of the eigenvalue problem (1) corresponding to the eigenfunctions displayed in Figures 3 and 4 (ordered left-to-right and top-to-bottom). All digits shown are believed correct on the basis of convergence analyses.

require use of sufficiently small contour regions—containing adequately small numbers of eigenvalues. These ideas suggest the development of an adaptive version of Algorithm 1 which is presented as Algorithm 2. This adaptive form of the method proceeds as follows. For complex (resp. real) eigenvalue searches, the algorithm subdivides space into adequately sized regions in the complex plane (resp. intervals in the real line) and then reapplies Algorithm 1 on a refined mesh in each smaller region. The recursion ends when the number of poles in a region does not change upon subdivision. The fact that Algorithm 1 is applicable to arbitrary curves is highly beneficial in this context, as the use of rectangular regions in the complex plane is well suited for the adaptivity purposes at hand. The pseudo-code for this modification is given in Algorithm 2.

It is important to mention that the AAA algorithm may fail to accurately produce the needed eigenvalues if the complex curve \mathcal{C} is not adequately resolved by the discretization provided by the set Z_N . An indication of insufficient resolution is the appearance of false poles (see [22]) near the curve \mathcal{C} , which in practice may be detected via an appropriate convergence analysis. Once an adequate resolution of \mathcal{C} is used, and provided the curve \mathcal{C} encloses a sufficiently small region in the complex plane, we have found in practice that, without exception, all eigenvalues with near machine precision accuracy can be obtained, following an initial application of AAA, by means of one of two possible methods, namely (i) Use of a subsequent “localized” AAA approximation applied to a few points around each eigenvalue obtained in the initial application of AAA; or, (ii) Use of the secant method applied to $1/S(k) = 1/u^*F_k^{-1}v$ starting at the eigenvalue obtained in the initial application of AAA. The numerical experiments in Section 6 illustrate the performance of Algorithm 2 augmented by means of each one of these localized accuracy-improvement procedures.

Eigenvectors corresponding to each eigenvalue can finally be obtained via evaluation, based on Gaussian elimination, of the nullspace of the matrix $F(k)$ at the approximated eigenvalues k . In detail, using Gaussian elimination with pivoting leads to an LU decomposition of the form $F(k) = LU$. Using this decomposition the nullspace of $F(k)$ can be computed by a simple two-step procedure consisting of (i) Selection of a set of canonical-basis vectors that are mapped to zero by the rows in the matrix U that are associated with the nonzero pivots; and, (ii) For each zero pivot in the matrix U , construction and solution of the reduced systems that result from the elimination of the rows and columns in U containing the zero pivots, and with right-hand sides equal to the negatives of each of the eliminated columns but excluding the column element in the eliminated row.

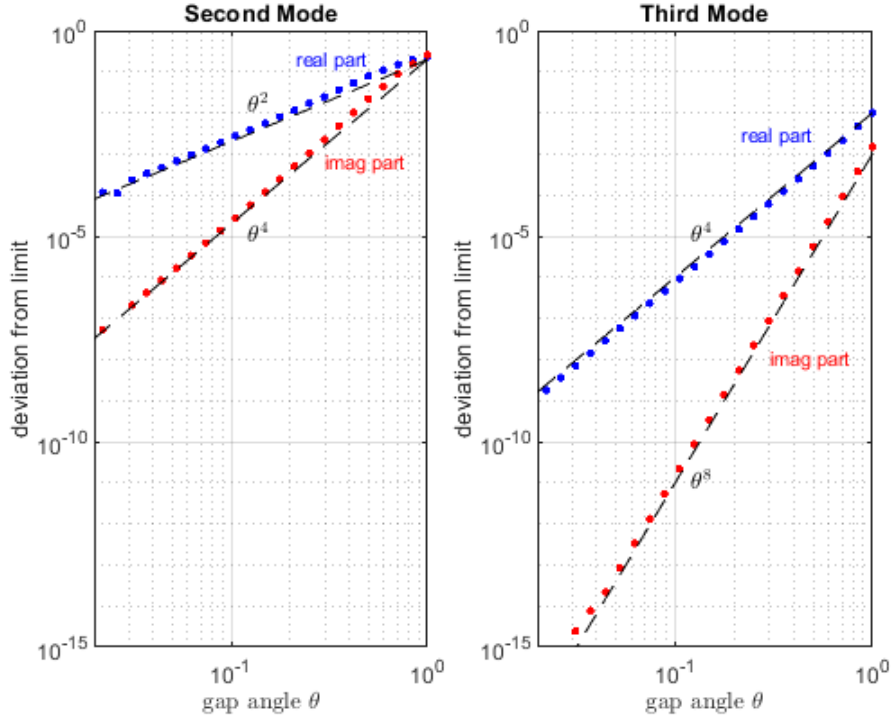


Figure 5: Convergence of $\Re(k)$ and $\Im(k)$ to their limiting values as the gap size θ shrinks to zero for the nearly degenerate open circle eigenfunctions displayed as the second and third images of Figure 4. For both modes the imaginary parts (decay rates) converge at double the rates of the real parts (spatial frequencies), and both the rates for the real and imaginary parts for the third mode are double those for the second mode. Note that for the third mode the approximate nodal line is aligned with the gap and thus results in a weaker coupling of interior and exterior fields and associated faster convergence.

6 Numerical Examples

A few numerical illustrations of the proposed methodology are presented in what follows, including a demonstration of the performance of Algorithm 2 on NEPs unrelated to Laplace eigenvalues (Section 6.1); a comparison of the proposed methods to approaches based on complex contour integration for NEPs in the context of Laplace eigenvalue problems (Section 6.2); a set of examples concerning Laplace eigenvalues and eigenfunctions for low and high frequencies and for open and closed arcs (Sections 6.3 and 6.5, respectively), and finally, an exploration of the rate at which scattering poles of open arcs converge to the corresponding interior eigenvalue as the opening closes.

6.1 Algorithm Verification on Two NEPs

This section illustrates the character of Algorithm 2 via applications to two problems included in the NLEVP collection [4], namely, the “CD player problem” and the “Butterfly problem”, whose eigenvalues are real in the first case, and complex in the second case. The CD player problem is an eigenvalue problem for a 60×60 matrix polynomial of the form $F(k) = k^2 I + k A_1 + A_0$ arising in the study of a CD-player control task [8]. We restrict attention to the interval $[-50, 5]$ on the real axis, within which the problem has 60 eigenvalues with absolute values as small as $2.23e - 4$ and as large as 41.1399; the real-interval

version of Algorithm 2 was used with a total number of 300 points k_j along each subinterval. The second problem is the butterfly problem, in which eigenvalues of a 64×64 matrix polynomial $F(k) = \sum_{i=0}^4 k^i A_i$ are sought. The matrices A_i are Kronecker products of linear combinations of the identity and nilpotent Jordan blocks [20]. We tackle the butterfly problem by employing Algorithm 2 applied initially to the box of side length 4 centered at the origin. This problem has 256 eigenvalues, and 100 values of k were used on each side of the square. Figure 1 displays the results produced by the proposed algorithm.

6.2 Comparison to a Contour Integration Method

In this section we compare our algorithm to the contour integration method of Beyn [5] (specifically ‘Integral Algorithm 2’) for solving NEPs, using the implementation given in [15]. The parameters for the integral equation algorithm were chosen based on [15, Lemma 2.13, Section 5]. For our test problem we compute scattering poles of the Dirichlet problem in the exterior of the unit circle C_1 , which are known analytically to equal the roots of the Hankel functions of the first kind [18]. In detail, this test seeks to produce the four scattering poles contained within the circular contour \mathcal{C} with center at $3 - 1.5i$ and radius 2, using both Algorithm 1 and Beyn’s method on the basis of equally spaced points along \mathcal{C} . The roots of Hankel functions are double, and we have found that neither Algorithm 1 nor Beyn’s method produce the eigenvalues to machine precision by evaluation along \mathcal{C} alone. Thus to improve accuracy we subsequently demonstrate the two different methods for accuracy refinement described in Section 5, namely, the secant method and the localized AAA approximation. Figure 2 demonstrates the performance of the various algorithms considered.

We emphasize that the same data, namely the scalarized resolvent $S(k)$ sampled at equally spaced points along the boundary of \mathcal{C} , was used to produce all of the non-localized results presented in Figure 2, suggesting certain advantages enjoyed by Algorithm 1 and its rational approximation-based eigenvalue search method. We have found that use of localized AAA approximations over a circle of radius $1e - 5$ works well in most situations. A localized calculation based on the secant method does not require parameter-tuning and it automatically provides an error estimate, however, which appears to make this localized approach preferable to the one based on AAA localization.

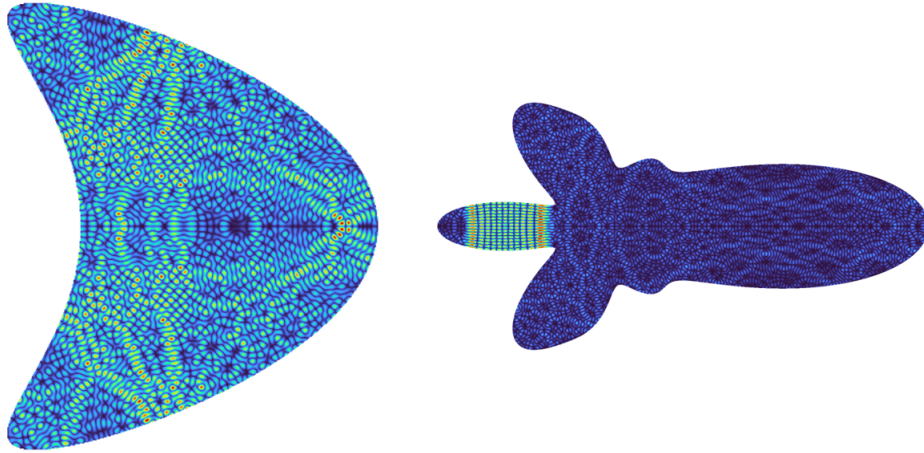


Figure 6: Left: Interior eigenfunction for the kite with eigenvalue 100.1846738596. Right: Interior eigenfunction for the rocket-shaped curve, with eigenvalue 399.9730212127. All digits shown were found to be correct by means of a convergence analysis.

6.3 Low-frequency Examples

This section considers eigenproblems related to the eigenfunctions displayed in Figures 3 and 4 and corresponding frequencies given in Table 1, namely, Laplace eigenvalues in the interior of a kite shaped domain (applying Algorithm 2 in a finite interval within the real axis), and open cavity eigenvalues for a circular cavity with an aperture of size $\pi/8$ radians, whose eigenvalues lie near the real axis (applying Algorithm 2 to a strip between the real axis and the complex point $-0.2i$). Since the strip is thin it suffices to apply the localization step by iteratively subdividing only the real part of the frequency domain.

6.4 Dependence on Gap Size

With a tool in hand to compute scattering poles quickly and accurately, certain mathematical aspects of their behavior may be considered, such as, e.g., the convergence rate of a complex scattering pole associated with a open arc equal to the difference between a closed curve and a gap section, as the gap size shrinks to zero. As an example we consider the second and third modes shown in the top row of Figure 4, and associated eigenvalues (but for varying gap sizes θ) which, for small θ are approximately equal to the lowest double eigenvalue the closed unit circle ($\theta = 0$)—namely the first root ≈ 3.8317 of the Bessel function $J_1(x)$. Figure 5 demonstrates the convergence of $\Re(k)$ (the “spatial frequency”) and $\Im(k)$ (the “decay rate”) to their limiting values as θ shrinks to zero. The combined set of convergence computations for the two modes considered was completed in approximately four seconds in single core of a present-day laptop computer.

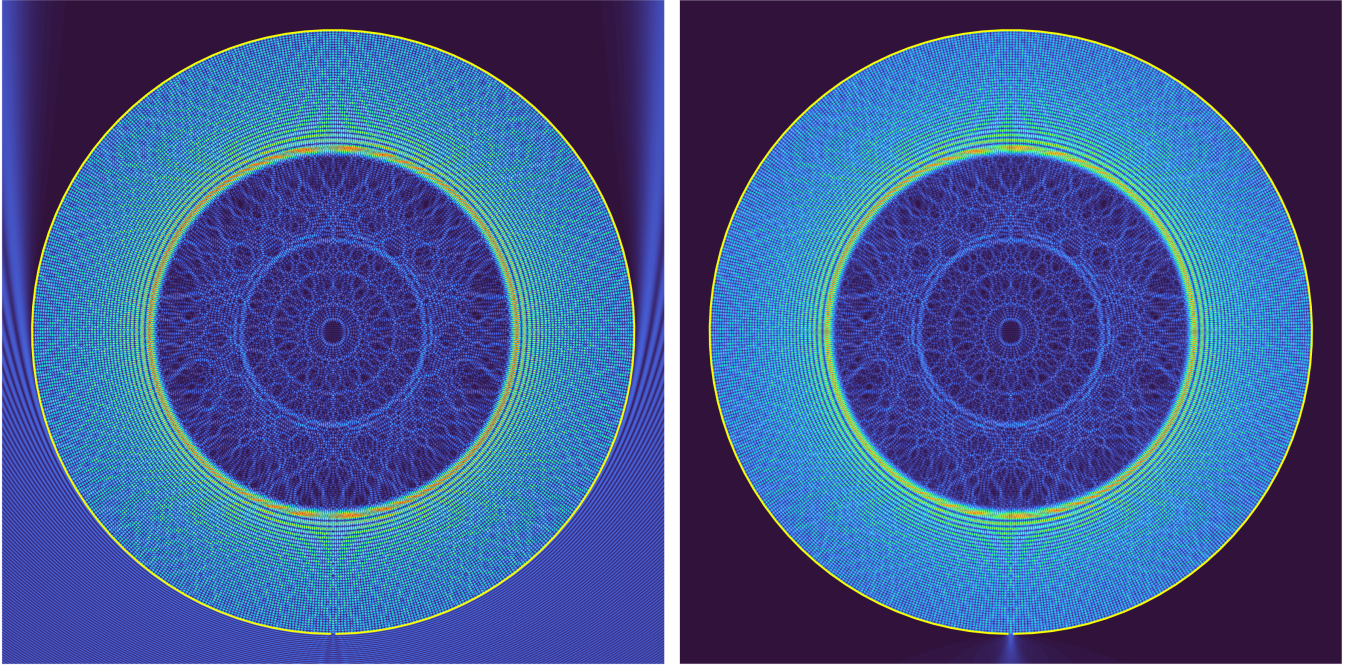


Figure 7: Comparison of the solution of the scattering problem with $k = 499.9073989141$ under vertical and upward plane-wave incidence (left) and the eigenfunction corresponding to the eigenvalue $499.9073989141 - 0.000779974959i$ (right) for an open circular cavity with aperture size $\pi/100$. All digits shown were found to be correct by means of a convergence analysis.

The first image in Figure 5 shows that for the second mode in Figure 4, whose convergence rate we presume to correspond to generic gap-shrinking eigenvalue convergence behavior, the frequency converges to its limiting value ≈ 3.8317 at the rate $O(\theta^2)$ and the decay rate to its limiting value 0 at the rate $O(\theta^4)$. For the third mode in the figure, in turn, the rates double to $O(\theta^4)$ and $O(\theta^8)$. This is related to the

alignment of the nodal line of the eigenfunction with the gap, which reduces the field coupling between the interior and exterior regions of the open cavity. We are not aware of any theoretical or computational studies reporting on such convergence rates for scattering poles as opening gaps tend to vanish.

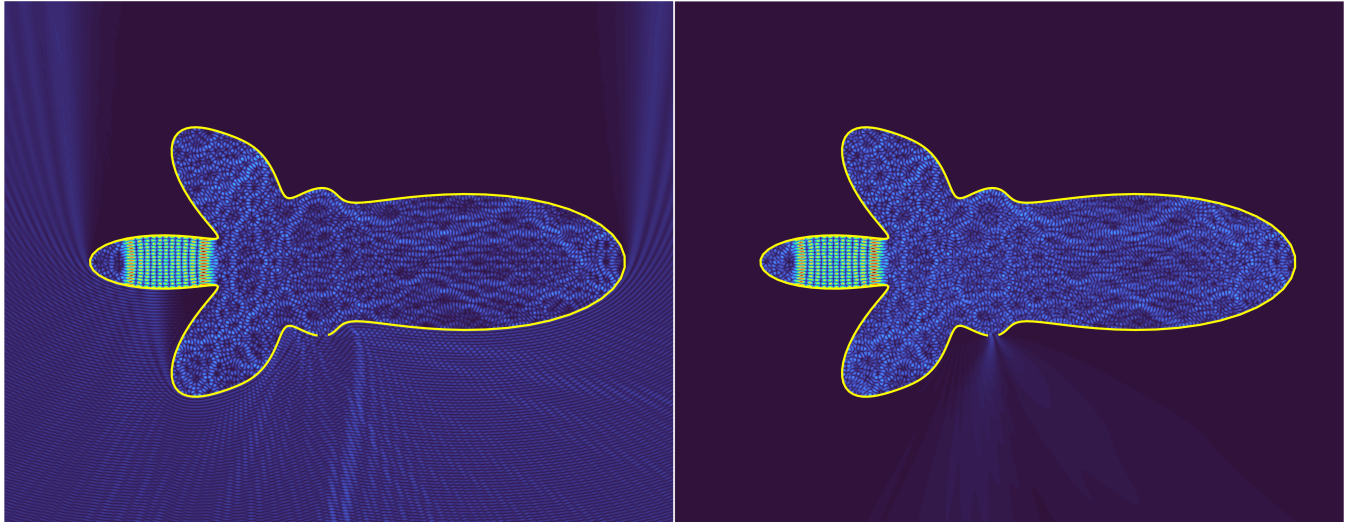


Figure 8: Comparison of the solution of the scattering problem with $k = 399.9694808817$ under vertical plane-wave incidence (left) and the eigenfunction corresponding to the eigenvalue $399.9694808817 - 0.00434495360i$ (right) for a rocket-like open cavity. The opening in the right curve is approximately equal to 0.6% of the curve length.

6.5 High-frequency Examples

Now we present several higher-frequency examples. To verify the accuracy of the proposed methods in high-frequency cases and in regions containing large numbers of eigenvalues we applied the real line version of algorithm 2 to obtain all 1244 interior Laplace eigenvalues of the unit circle that are contained in the interval $[1, 100]$. The algorithm automatically obtained to all 1244 eigenvalues with near machine accuracy in an average computational time of 1.09 seconds per eigenvalue in a single CPU core. This relatively slow figure is dominated by the higher eigenvalues; for example the average time per eigenvalue in the interval $[0, 25]$ is only about 0.079 seconds.

Having verified our algorithm in the high-frequency regime, we subsequently applied the proposed methods to several high-frequency eigenvalue problems for interior and open-cavity domains. Figure 6 displays high-frequency interior eigenfunctions for kite-shaped and rocket-shaped cavities. The right panels in Figures 7 and 8, in turn, present eigenfunctions for circular and rocket-shaped open cavities, while the left panels of these figures present the solutions of problems of scattering by the same cavities under vertical upward-facing plane-wave illumination. Clearly, the left panel scattering solutions display a close resemblance with the eigenfunctions displayed in the right panels, evidently suggesting that the open-cavity eigenfunctions can be excited by adequately oriented incident fields penetrating through the small apertures. All digits displayed in the figure captions have been found to be exact by means of studies of convergence analysis in both the discretization of the integral equations used and of the eigensearch algorithms utilized.

7 Conclusions

This paper introduced a novel numerical algorithm for the evaluation of real and complex eigenvalues and eigenfunctions of general NEPs, including NEPs associated with Laplace eigenvalue and scattering-

resonance problems for open and closed domains. Based on use of adaptive eigenvalue search methods based on either AAA rational approximation or AAA approximation combined with secant-method refinement, the algorithm produces highly accurate eigenpairs for challenging eigenproblems at both low and high frequencies alike. Comparisons with a well-known contour-integration method demonstrated a number of advantages of the proposed approach, including fast convergence and ease of applicability on non-smooth contours. The latter characteristic is significant, in that it greatly facilitates use of the algorithm in a rectangular refinement-based adaptive strategy—resulting in automatic evaluation of all eigenvalues contained within a given region with near machine precision accuracy.

Acknowledgements

This material is based upon work supported by the National Science Foundation Graduate Research Fellowship under Grant No. 2139433. OB gratefully acknowledges support from NSF and AFOSR under contracts DMS-2109831 and FA9550-21-1-0373.

References

- [1] Eldar Akhmetgaliyev and Oscar P. Bruno. Regularized integral formulation of mixed Dirichlet-Neumann problems. *J. Integral Equations Applications*, 29:493–529, 2017.
- [2] Eldar Akhmetgaliyev, Oscar P. Bruno, and Nilima Nigam. A boundary integral algorithm for the Laplace Dirichlet–Neumann mixed eigenvalue problem. *Journal of Computational Physics*, 298:1–28, 2015.
- [3] Carlos J.S. Alves and Pedro R.S. Antunes. Wave scattering problems in exterior domains with the method of fundamental solutions. *Numerische Mathematik*, 156:1–20, 2024.
- [4] Timo Betcke, Nicholas J Higham, Volker Mehrmann, Christian Schröder, and Françoise Tisseur. NLEVP: A collection of nonlinear eigenvalue problems. *ACM Transactions on Mathematical Software (TOMS)*, 39(2):1–28, 2013.
- [5] Wolf-Jürgen Beyn. An integral method for solving nonlinear eigenvalue problems. *Linear Algebra and its Applications*, 436(10):3839–3863, 2012.
- [6] Oscar P. Bruno and Stéphane K. Lintner. Second-kind integral solvers for TE and TM problems of diffraction by open arcs. *Radio Science*, 47(06):1–13, 2012.
- [7] Oscar P. Bruno and Stéphane K. Lintner. A high-order integral solver for scalar problems of diffraction by screens and apertures in three-dimensional space. *Journal of Computational Physics*, 252:250–274, 2013.
- [8] Younes Chahlaoui and Paul Van Dooren. A collection of benchmark examples for model reduction of linear time invariant dynamical systems. *EPrint 2008.22, Manchester Institute for Mathematical Sciences, University of Manchester, Manchester*, 2002.
- [9] David L. Colton and Rainer Kress. *Integral Equation Methods in Scattering Theory*. Pure and Applied Mathematics. John Wiley & Sons Inc., New York, 1983.
- [10] David L. Colton and Rainer Kress. *Inverse acoustic and electromagnetic scattering theory, 4th Edition*. Springer, 2019.
- [11] Tobin A. Driscoll, Nicholas Hale, and Lloyd N. Trefethen. Chebfun guide, 2014. www.chebfun.org.

- [12] Mohamed El-Guide, Agnieszka Międlar, and Yousef Saad. A rational approximation method for solving acoustic nonlinear eigenvalue problems. *Engineering Analysis with Boundary Elements*, 111:44–54, 2020.
- [13] Steven Elsworth and Stefan Güttel. Conversions between barycentric, RKFUN, and Newton representations of rational interpolants. *Linear Algebra and its Applications*, 576:246–257, 2019.
- [14] Stefan Güttel, Gian Maria Negri Porzio, and Françoise Tisseur. Robust rational approximations of nonlinear eigenvalue problems. *SIAM Journal on Scientific Computing*, 44(4):A2439–A2463, 2022.
- [15] Stefan Güttel and Françoise Tisseur. The nonlinear eigenvalue problem. *Acta Numerica*, 26:1–94, 2017.
- [16] Pieter Lietaert, Karl Meerbergen, Javier Pérez, and Bart Vandereycken. Automatic rational approximation and linearization of nonlinear eigenvalue problems. *IMA Journal of Numerical Analysis*, 42(2):1087–1115, 2022.
- [17] Stéphane K. Lintner and Oscar P. Bruno. A generalized Calderón formula for open-arc diffraction problems: theoretical considerations. *Proceedings of the Royal Society of Edinburgh*, 145(2):331–364, 2015.
- [18] Yunyun Ma and Jiguang Sun. Computation of scattering poles using boundary integrals. *Applied Mathematics Letters*, 146:108792, 2023.
- [19] William Charles Hector McLean. *Strongly elliptic systems and boundary integral equations*. Cambridge University Press, 2000.
- [20] Volker Mehrmann and David Watkins. Polynomial eigenvalue problems with Hamiltonian structure. *Electronic Transactions on Numerical Analysis*, 13:106–118, 2002.
- [21] Ryota Misawa, Kazuki Niino, and Naoshi Nishimura. Boundary integral equations for calculating complex eigenvalues of transmission problems. *SIAM Journal on Applied Mathematics*, 77(2):770–788, 2017.
- [22] Yuji Nakatsukasa, Olivier Sète, and Lloyd N. Trefethen. The AAA algorithm for rational approximation. *SIAM Journal on Scientific Computing*, 40(3):A1494–A1522, 2018.
- [23] Yousef Saad, Mohamed El-Guide, and Agnieszka Międlar. A rational approximation method for the nonlinear eigenvalue problem. *arXiv preprint arXiv:1901.01188*, 2019.
- [24] Olaf Steinbach and Gerhard Unger. Convergence analysis of a Galerkin boundary element method for the Dirichlet Laplacian eigenvalue problem. *SIAM Journal on Numerical Analysis*, 50(2):710–728, 2012.
- [25] Michael E. Taylor. *Partial differential equations. II*. Springer-Verlag, New York, 1996.
- [26] Lin Zhao and Alex Barnett. Robust and efficient solution of the drum problem via Nyström approximation of the Fredholm determinant. *SIAM Journal on Numerical Analysis*, 53(4):1984–2007, 2015.